



# A novel trench fibre push-out method to evaluate interfacial failure in long fibre composites

Robin M. G. De Meyere<sup>1,a)</sup> , Kay Song<sup>2</sup>, Louise Gale<sup>3</sup>, Stephen Harris<sup>3</sup>, Ian M. Edmonds<sup>3</sup>, Thomas J. Marrow<sup>1</sup>, Eduardo Saiz<sup>4</sup>, Finn Giuliani<sup>4</sup>, David E. J. Armstrong<sup>1</sup>, Oriol Gavaldà-Diaz<sup>4</sup>

<sup>1</sup> Department of Materials, University of Oxford, Oxford OX1 3PH, UK

<sup>2</sup> Department of Engineering Science, University of Oxford, Oxford OX1 3PJ, UK

<sup>3</sup> Rolls-Royce Plc, Derby DE24 8BJ, UK

<sup>4</sup> Centre for Advanced Structural Ceramics, Department of Materials, Imperial College London, London SW72AZ, UK

<sup>a)</sup> Address all correspondence to this author. e-mail: robin.demeyere@seh.ox.ac.uk

Received: 13 November 2020; accepted: 2 March 2021; published online: 23 March 2021

**Traditional fibre push-outs for the evaluation of interfacial properties in long fibre ceramic matrix composites present their limitations—solutions for which are addressed in this work by introducing the novel trench push-out test. The trench push-out makes use of a FIB milling system and an SEM in-situ nanoindenter to probe a fibre pushed into a trench underneath, allowing in-situ observations to be directly correlated with micromechanical events. SiC<sub>f</sub>/BN/SiC composites—candidate material for turbine engines—were used as model materials in this work. Different fibre types (Hi-Nicalon and Tyranno type SA3) were coated with BN interphases, presenting mean interfacial shear stresses of 14 ± 7 MPa and 20 ± 2 MPa, respectively, during fibre sliding. The micromechanical technique enabled visualisation of how defects in the interphase (voids, inclusions & milled notches) or in the fibre (surface asperities, non-uniform coatings) affected the variability of interfacial property measurement.**

## Introduction

CMC (Ceramic Matrix Composites) consist of ceramic fibres imbedded in a ceramic matrix, bonded by an interphase. The reliability and predictability of CMC properties are major obstacles to their immediate implementation in aerospace and nuclear industries. The CMC fibre (weave-level) macrostructures demonstrate complexity, and their toughening mechanisms at the microstructural scale are not fully understood [1]. The SiC/SiC CMCs used in this study are candidate materials for combustion chambers, vanes, seal segments and shroud components in engines [2]—but CMC lifing models are currently limited by the lack of inputs and the difficulty in measuring repeatable interfacial material properties.

The BN interphase between the SiC fibres and matrix is key to the apparent toughness of the composite. Indeed, cracks are able to deflect and fibres can pull-out, thus increasing the fracture toughness of monolithic SiC [3] from 2–3 to 15–20 MPa m<sup>1/2</sup> in the composite [4] form. When investigating the oxidation resistance properties of the CMC, outside

debonding (cracks propagating at the SiC<sub>m</sub>/BN interface) produces a more resistant material than inside debonding (cracks propagating at the SiC<sub>f</sub>/BN interface) [5]. Indeed, inside debonding reduces the stress oxidation capabilities of the composite due to the delayed exposure of the fibres to the environment [5, 6]. Crack deflections at BN interphases are more likely to occur at the inner SiC<sub>f</sub>/BN interface than at the outer SiC<sub>m</sub>/BN interface due to the differences in stiffness ratios [7–9]. If SiC fibres are too strongly bonded to the interphase they fail in a brittle manner and come short of providing adequate toughness [10]. Indeed, ‘strongly’ bonded fibres fail without promoting crack deflection, thus preventing associated toughening mechanism such as fibre bridging [11]. This mechanism is in contrast to other failures whereby fibres are either adequately bonded to the interphase and cracks propagate within the BN (cohesive failure). In the event that the interphase is weakly bonded, cracks are able to propagate along the fibre/BN interface or the matrix/BN interface (adhesive failure) for pull-out.

Micro-scale techniques have helped bridge the gap between explaining atomic and molecular scale events and macro/

mesoscale mechanics. The micropillar compression technique applied to SiC<sub>f</sub>/PyC/SiC was investigated by Kabel et al. [1] extensively but that study presented its limitations, as pillars can often be too fragile and experience instant debonding. Furthermore, Kabel et al. iterate that no kinetic properties (e.g. load rate effects) can be obtained reliably from the stage after debonding and cracks cannot be propagated in a stable manner. On the other hand, fibre push-outs—first theorised by Marshall in 1985 and performed in 1987 by Marshall & Oliver [12]—best mimic the mechanisms of CMC failure and can provide a measurement of the interfacial shear stress (ISS)  $\tau$  experienced at the interphase, which is estimated by [13]:

$$\tau = \frac{F}{2\pi RH} \quad (1)$$

where  $F$  is the push-out load,  $R$  is the fibre radius and  $H$  the sample thickness. Sample thinning to appropriate dimensions (where the tow architecture influence is reduced and where push-out load is lower than the load-cell limit of the mechanical device) is required—usually to sample thicknesses not exceeding 100  $\mu\text{m}$  [14]. Sample thinning is challenging due to the hardness and brittleness of the ceramic composites.

The difficulty of sample preparation for the fibre push-out was illustrated by both works of Boakye et al. [15] making use of a tripod polisher and a light microscope to manually correct for fibre alignment with respect to the polished surface, and works by Herbreteau et al. [16] whom used wedge designs and ion slicers. The loading during fibre push-out can have further effects such as bending of the specimen or the holder, which can prevent accurate measurements. Ideally, a flat-punch nanoindentation tip is used to prevent fibre damage [17]; however, even flat-punch tips have been known to leave an impression on the fibre surface due to the large force needed [18]. It was shown by Mueller et al [18] that load/displacement curves are significantly different from Berkovich push-out and that a parallel alignment of the tip and fibres surface is necessary to minimise the impact of sharper indenters. Moreover, Kabel et al. [1] highlighted that poor calibration of the microscope-to-indenter positioning can result in lower throughput and technique yields, as the experimental acquisition is slowed down.

A major limitation of the fibre push-out method lies in the lack of information regarding in-situ observations, as the fibre is fully imbedded in the matrix. This results in little knowledge on how defects in the matrix (voids, inclusions, chemical segregations) or in the fibre (surface asperities, non-uniform coatings, pre-mature oxidation) affect the variability of interfacial property measurements. Even if tested in an SEM, there is no direct visualisation of either crack(s) propagating or the dominating failure mechanism (e.g. cohesive failure or nature of debonding). Simultaneous observations of the said mechanism and the artefacts at the top and bottom of the fibre are needed for a full

understanding of the test results. Furthermore, mechanical data obtained from traditional fibre push-outs show a high degree of variability, which can be alleviated and better understood with the use of novel in-situ techniques.

Another key concern lies in how the push-out technique can be representative and replicate material behaviour in its proposed application. The data analysis for fibre push-out is particularly challenging as it is usually performed post-mortem as opposed to in-situ, which can lead to potential errors in data matching (associating a specific fibre to a load/displacement curve and an SEM micrograph of failure for example). There is a need to develop a micromechanical technique that can extract the micromechanical properties of the composite interphase reliably and in a reproducible manner. The trench push-out technique introduced in this work aims to address some of these issues for a future better understanding of how processing, degradation or other factors affect composite performance [19].

## Results

Due to the uncertainties surrounding fibre push-outs performed ex-situ, an SEM in-situ technique that enabled visualisation of small-scale events has been proposed. A novel ‘trench push-out’ method depicted in Fig. 1 has been adapted from the similar trench micropillars by Wu et al. [30] whom performed tests on electrical VIA’s (Vertical Interconnect Access). More detail on technique preparation and the material used in this study are included in the methods section.

The ISS  $\tau$  at peak load (maximum load) and plateau load (purely frictional) were calculated with Eq. (1) for full fibres and Eq. (2) for half fibres.

$$\tau = \frac{F}{\pi RH} \quad (2)$$

A standard load/displacement curve and corresponding SEM frame from a half fibre trench push-out is shown in Fig. 2. The load–displacement curve is similar to traditional push-out responses in displacement control: a peak in load is observed before full crack propagation [19, 20], after which a plateau load shows the fibre sliding into the trench.

Testing of fibres at the edge of tows or closer to the edge of the trench, as seen in Fig. 2b, results in a tendency for the load to increase at the end of the plateau (past point (3) on Fig. 2a where the tip cone starts making contact with the top outskirts of the fibre). The sharp load-drop from point (1) to point (2) in displacement-controlled experiments corresponds to crack(s) fully propagating and leading to fibre sliding. Looking in more detail at a sequence of SEM images from a trench push-out test of a half fibre (Fig. 3) shows that transverse radial cracks first propagate in the CVI SiC surrounding the fibre (3(b), 3(c)). Thereafter, coils of BN interphase emerge at the surface (3b).

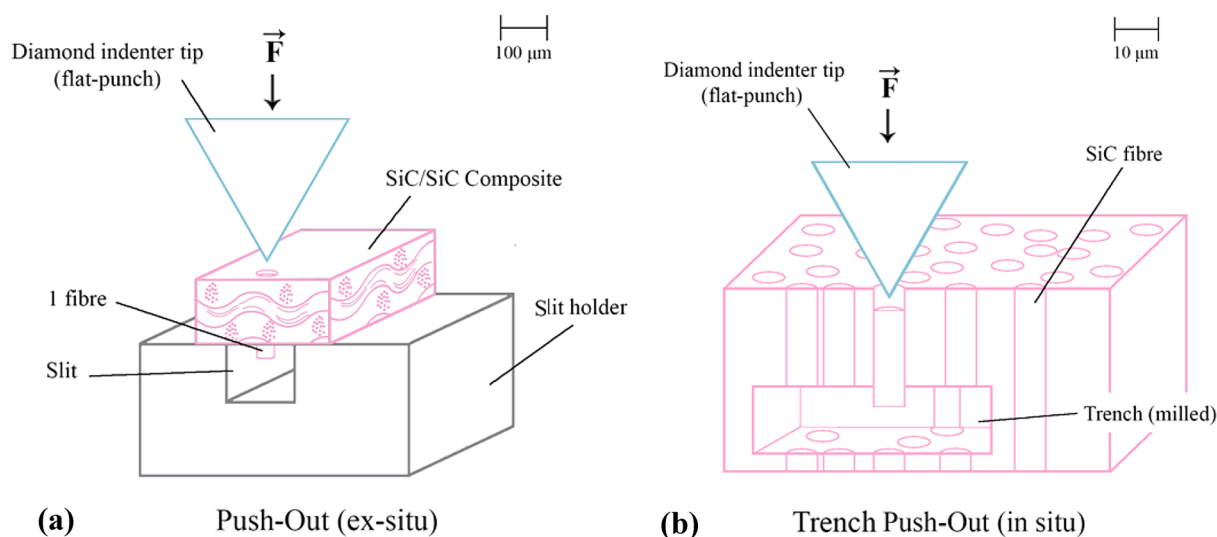


**Figure 1:** (a) Ex-situ push-outs and (b) novel SEM in-situ trench push-outs. The SiC/SiC composite (and fibre) in a) have been enhanced for clarity and are not to exact scale with the corresponding scale bar.

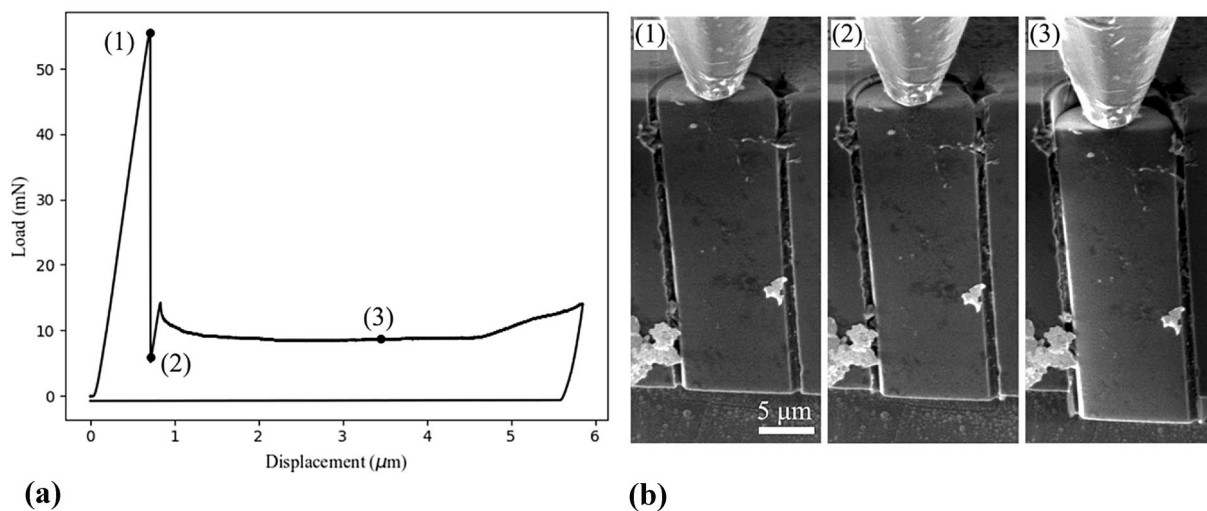


**Figure 2:** (a) Load–displacement curve and corresponding (b) SEM frame from an in-situ trench push-out experiment conducted on a Hi-Nicalon fibre.

Radial cracks in the CVI SiC propagate until the fibre—alongside the BN and part of the CVI SiC—is pushed inside the trench towards the end of the test (3d).

The frictional degradation with the BN interphase coils and subsequent resurfacing is visible on Fig. 3b. Cracks have also propagated to neighbouring fibres and neighbouring interphases in the transverse direction as shown in Fig. 3d.

When testing full fibres directly beneath the trench or with no trench on fully pushed out samples (Fig. 4), an increase in the load response towards the end of the test from tip/material contact—akin to that of past point (3) in Fig. 2a—was observed.

Looking at the magnitude of plateau loads obtained during the trench push-outs in Table S1—loads found on half fibres

were almost half those found on full fibres. When calculating shear stresses using Eq. (1) comparing the half and full fibres, similar stresses were obtained on the same sample. The accuracy and error on these measurements are taken into consideration in the discussion.

The pushing out of two neighbouring Hi-Nicalon fibres on Fig. 5 suggests there was strong adhesion between fibres and that the adhesive strength between fibres was greater than the fibre/interphase bonding. This suggests that the interphase bond between fibres is not homogeneous, with some fibres touching each other and transferring load between one another.

It was observed that sample preparation induced defects in the interphase: for example, different trench-milling rates

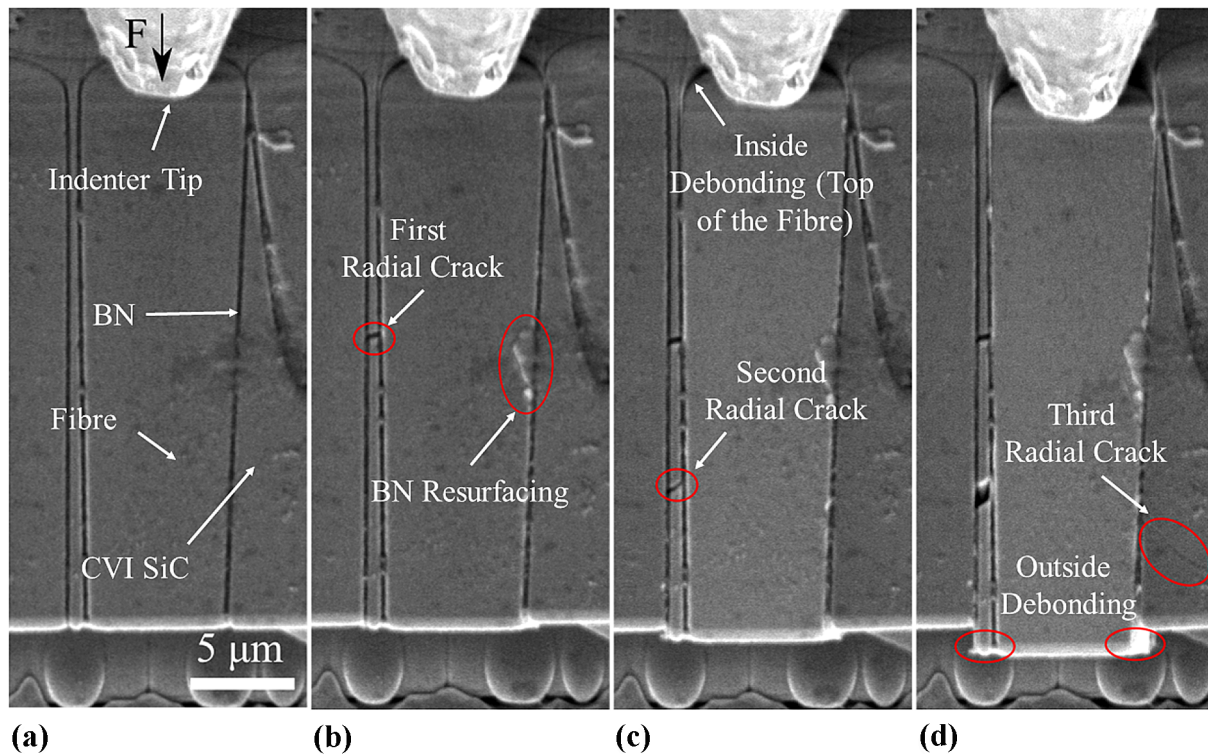


**Figure 3:** SEM frames from an in-situ trench push-out experiment on the SiC<sub>f</sub>/BN/SiC sample with Hi-Nicalon fibres showing progressive cracks in the surrounding CVI SiC, the BN coiling and resurfacing, and both the BN and the CVI SiC pushing out at the bottom of the sample inside the trench.

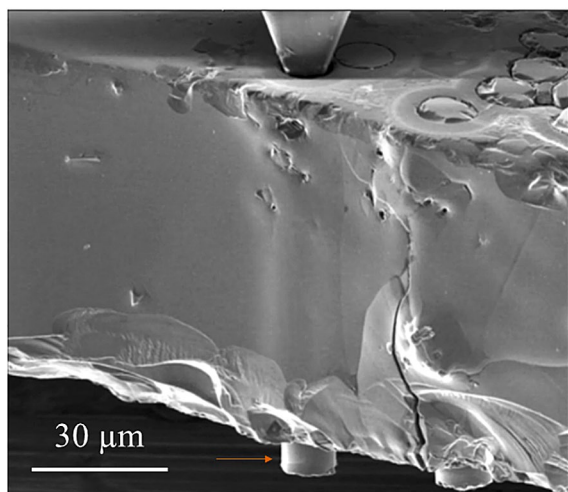


**Figure 4:** SEM frame from an in-situ push-out experiment on the SiC<sub>f</sub>/BN/SiC sample with Hi-Nicalon fibres showing a loading of a traditional push-out with the fibre protruding from the bottom (orange arrow), but no visual information on the micromechanical events is given.

for the SiC and BN might have resulted in preferential milling and notched areas in the SiC and BN at the bottom of the fibre. Diagonal cracks with respect to loading direction were observed to have propagated from the bottom and connected pre-existing pores as seen on Fig. 6. Similar observations were

made in samples with pre-existing defects from manufacturing (e.g. non-homogeneous coatings). In this context, the SEM frames on Fig. 6 show that (i) cracks initiate towards the bottom half of the fibre (close to the trench) and propagate upwards to the tip, and (ii) cracks have propagated between the fibres and the interphases as remnants of both Boron and Nitrogen are visible on EDX on the bare top section of the push-out as highlighted in Fig. 7. The visualisation of pre-existing defects in the BN interphase and how they interact with the cracks help explain any outlier values in the loads recorded whilst reducing variability in the stresses recorded.

When comparing the different fibre types, the Tyranno type SA3 fibres exhibited the same behaviour: a mix of both inside and outside debonding illustrated in Fig. 8. Simultaneous failures occurred, the BN was left untouched at the fibre top close to the tip (inside debonding), whilst concurrently adhering to the bottom of the fibre being pushed in the trench (outside debonding). The crack propagation behaviour is investigated in the discussion.

The loads obtained from the frictional section of the tests (as the fibres were sliding) were used to calculate ISS, and compared to the fibre roughness data acquired with the triboindenter in Table S2.

The debonding load and shear stresses refer to the max loading point before catastrophic crack propagation and

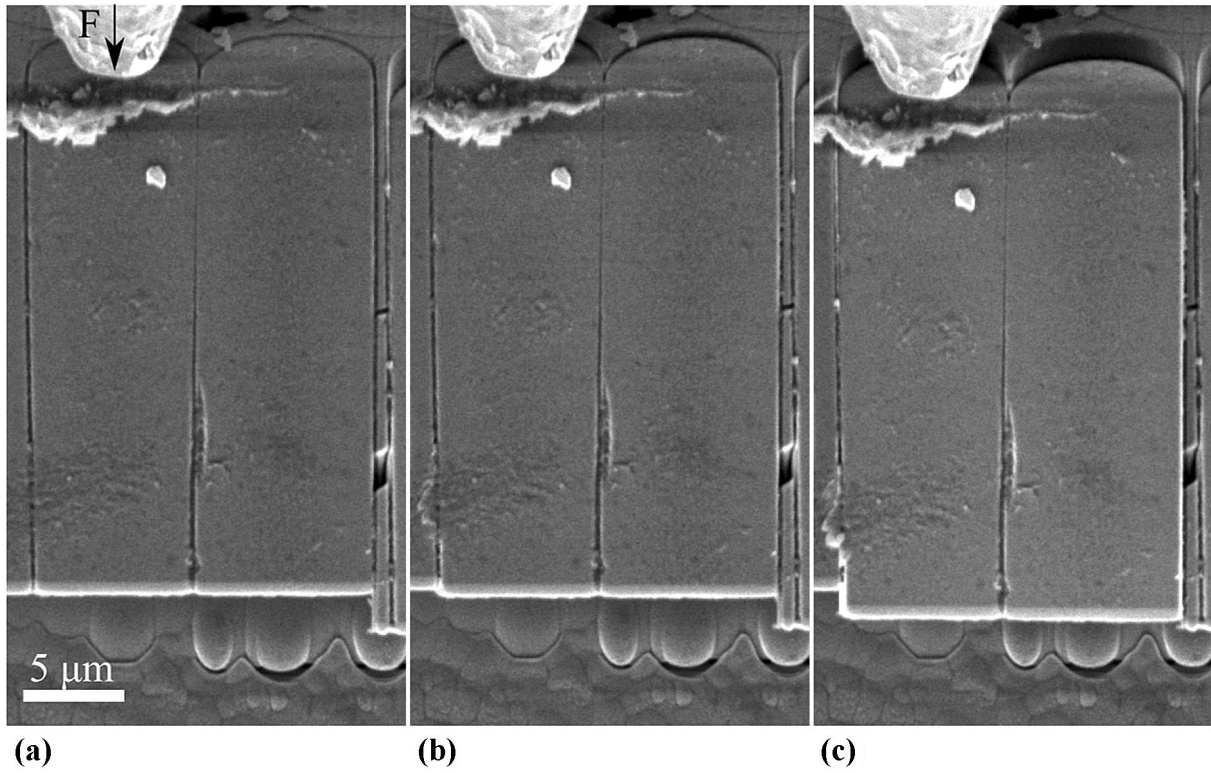


**Figure 5:** SEM frames from in-situ trench push-out experiments on the SiC<sub>f</sub>/BN/SiC sample with Hi-Nicalon fibres showing loading of 2 half fibres simultaneously.

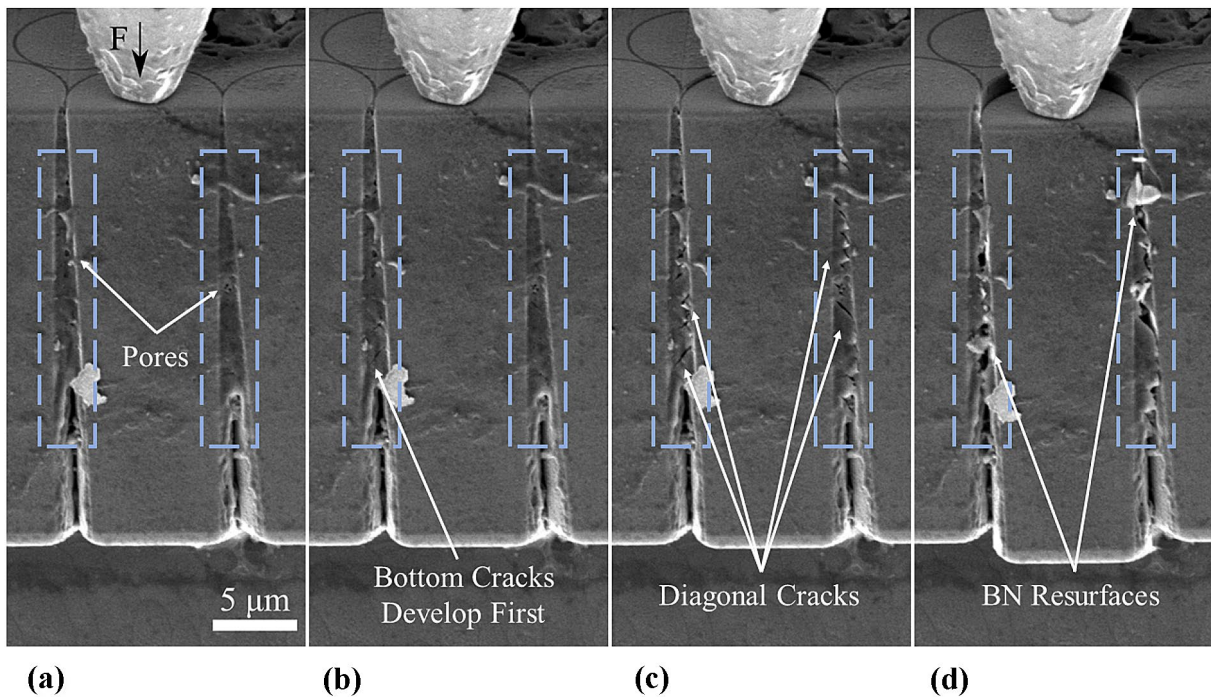


**Figure 6:** SEM frames from an in-situ trench push-out experiment on the SiC<sub>f</sub>/BN/SiC sample with Hi-Nicalon fibres showing gradual formation of diagonal tracks, from bottom to top inside the BN, as cracks connect pre-existing pores and defects in the interphase.

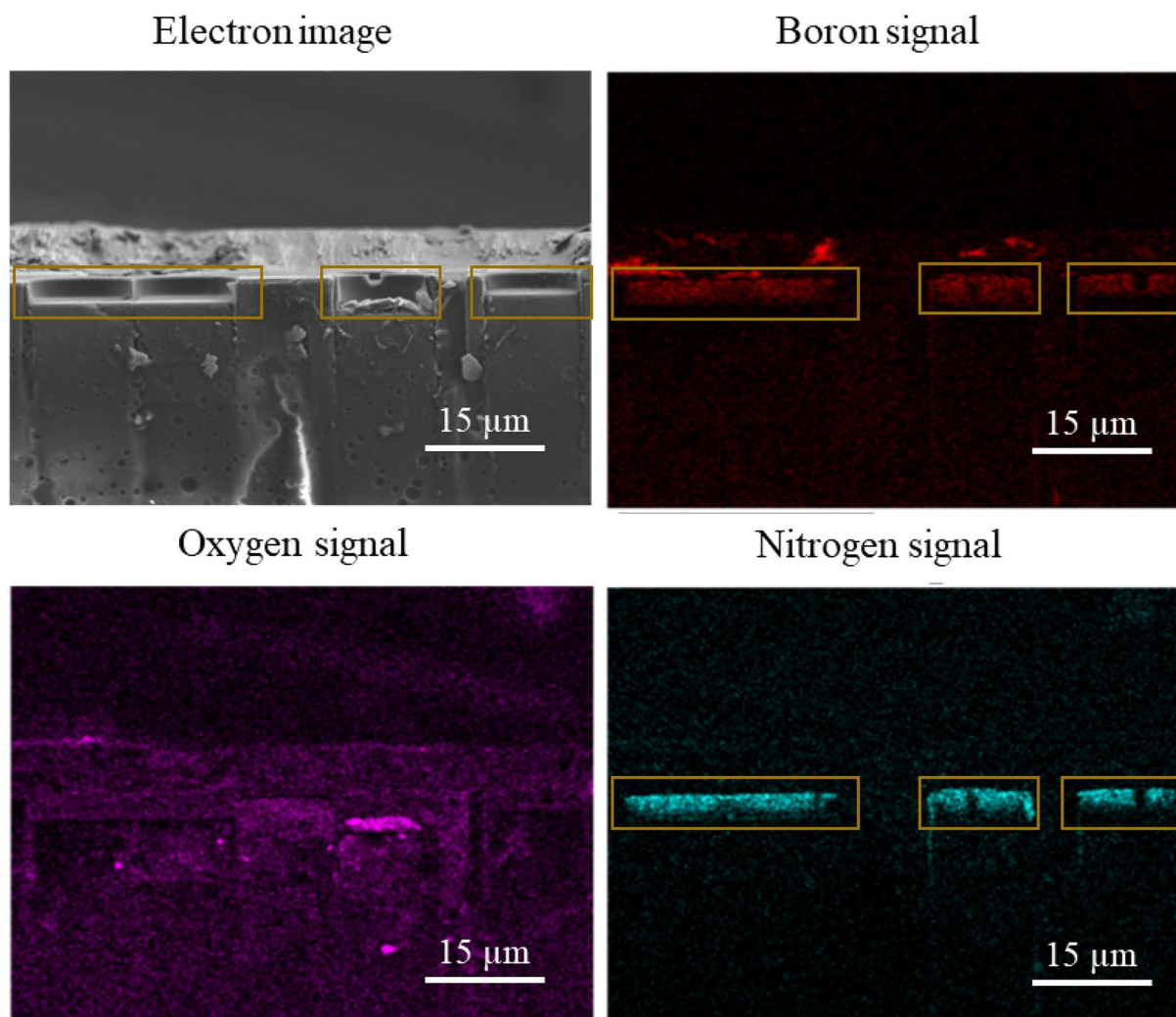


**Figure 7:** SEM EDX analysis of tested half fibres showing BN signals (inside the golden squares) on the denuded top edges of Hi-Nicalon fibres. Circular defects on the fibre surface stem from sample cleaning after testing.

initiation of fibre sliding (the maximum loading point on F2). Table S2 mean values gave insights to compare the two fibre types tested. The higher roughness of the Tyranno type SA3 fibres ( $100 \pm 5$  nm) resulted in stronger mechanical properties overall. A significantly larger stress from fibre sliding for the Tyranno type SA3 fibre once the crack fully propagated was observed. Similarly, the stress required to debond the fibre was more significant as the BN interphase might have had additional mechanical keying when deposited on a rougher fibre surface. It is worthwhile noting that the maximum shear stress before fibre sliding was much higher for the Hi-Nicalon fibres despite the rougher Tyranno type SA3 fibres. During sliding of half fibres, only half of the surface could contribute to resisting the push-out, suggesting the interphase friction coefficient was the biggest contributor to slowing crack propagation at the later stages of the micromechanical test.

## Discussion

From an experimental point-of-view, the half fibres show promise as model material for micromechanical testing. Half fibres (or any partial fibre in general) are indeed easier to mill (as milling depths for the trenches are reduced to only half fibre radii), and can display clear crack trajectories when tested in-situ. The comparison between half and full fibre tests showed similar values ( $23.8 \pm 0.4$  and  $24.6 \pm 0.4$  MPa, respectively) for the frictional ISS measured—thus demonstrating the viability in pushing half fibres on the surface near the edge of the trench on the polished side. These values are further comparable to ISS measurements of  $28 \pm 7$  MPa made using more traditional push-outs (through thickness) performed on the same material [21]. In the context of half (or incomplete fibres), the residual stresses released from

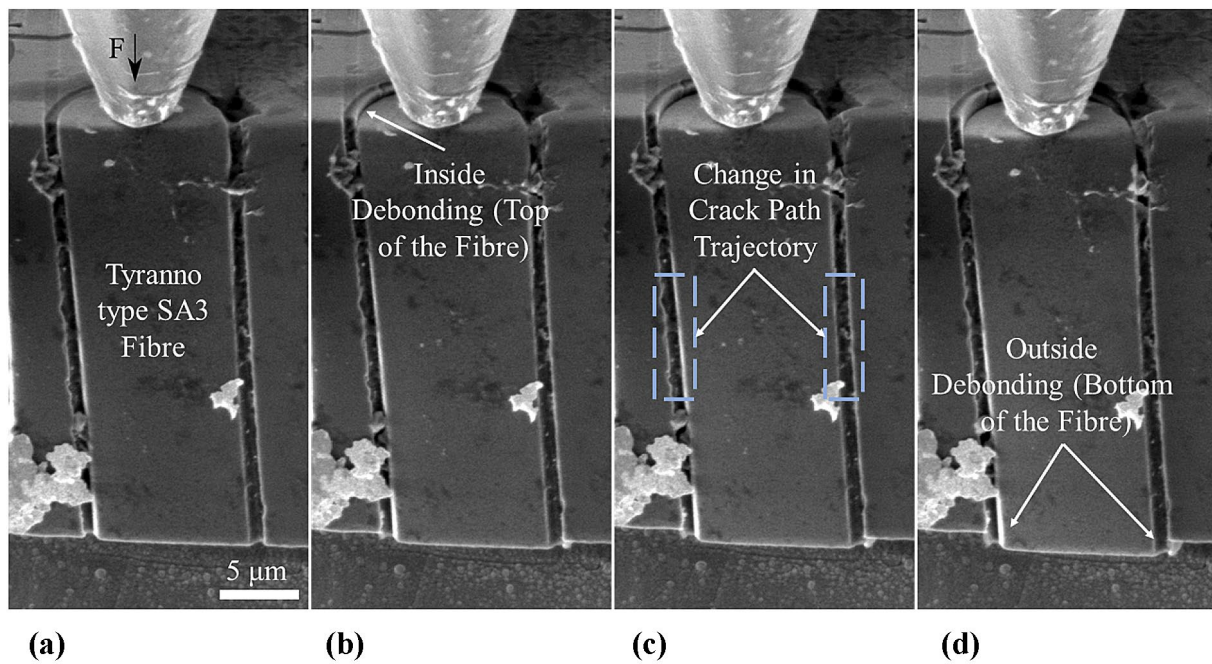


**Figure 8:** SEM frames from an in-situ trench push-out experiment on the SiC/BN/SiC sample with Tyranno type SA3 fibres showing simultaneous inside debonding (top) and outside debonding (bottom as BN is pulled out) suggesting there are two changes in crack propagation modes after the crack(s) initiate(s).

the ‘free boundary’ at the sample edge have no visible effects on the remaining BN interphase coating the half fibre.

Fibre types and their adherence to coatings were compared with the use of trench push-outs. The EDX studies (Fig. 7) showed the BN on the top Hi-Nicalon fibre surface after push-out. This suggested inside debonding dominated with the crack propagating between the BN interphase and the fibre. The inside debonding on the top surface of the fibres was also observed by other works on traditional push-outs [6, 17, 22], however, limited to no events on the bottom half of the fibres were reported with traditional push-outs (i.e. samples were not flipped and examined post-mortem). Since orthogonal cracks—perpendicular to the axial direction of the fibres—also propagated (Figs. 3 and 6), both inside debonding and a subsequent relaxation of residual hoop stresses in the fibre environment was likely to have occurred. It was also observed that for both Hi-Nicalon and Tyranno type SA3 fibres, a significant portion of the BN interphase remained attached to the fibre during push-out (Fig. 8d). A possible explanation lies in the interphase oxidising through Oxygen ingress during fabrication or sample preparation, thereby increasing the strength of the fibre/BN interface bonding. Alternatively, increased mechanical keying (especially if the fibres were attached together) can be observed as a result of a heterogeneous defect distribution in the interphase prior to testing. Tyranno type SA3 fibres also showed a mixture of failure modes during the same test as shown on Fig. 8 where both inside and outside debonding mechanisms occurred. Despite

the ratio of roughnesses of the two fibre types, the Hi-Nicalon fibres on average displayed significantly higher shear stresses at maximum load only, as seen in TABLE S2. This may be due to the thinner BN coating on the Hi-Nicalon samples having better adhesion, as the driving force for cracking and delamination increases with thickness [23]. The fibre roughness measurements are in line with both these results and literature [24–26] where Tyranno fibres are rougher—regardless of their generation—on the surface than their Hi-Nicalon counterparts, resulting in higher shear stresses measured.

One of the key advantages of the trench push-out is the possible visualisation, explanation and correlation of the crack path to corresponding micromechanical events. In Hi-Nicalon fibre tests such as the one shown in Fig. 3, cracks seemed to initiate in the neighbouring CVI SiC and/or SiC matrix, before radially propagating from the loading direction. These secondary cracks may be induced due to the relaxation of stresses neighbouring the fibre being tested as highlighted by Hull et al. [12], their direction can be attributed to the columnar microstructure of the CVI SiC with grains aligned radially from the fibres as highlighted by Gavalda-Diaz et al [19, 27]. In a more realistic context for gas turbine engines, fibre pull-out (as opposed to push-out) would induce a slight fibre shrinkage from Poisson contraction, thus decreasing the radial force acting on the BN/fibre bond, resulting in less damage on the surrounding CVI SiC. The porosity and quality of the BN interphase induced diagonal cracks (Fig. 6) within the interphase, which then interconnected

to enable a larger longitudinal (alongside fibre direction) crack to fully propagate and the fibre to push-out. The BN porosity has previously been linked to increased rate of oxidation in both its monolithic [28] and composite form [29]. Experiments with a higher density of fibres in the tow (Fig. 6) show that cracks had a tendency to propagate at the fibre BN interface whilst those with a lower density (Fig. 3) show cracks propagating in the CVI SiC between fibres. This shows that fibre packing has a strong influence on crack path trajectory, and this can be investigated using this technique. Even if the fibre packing density is too elevated, testing of full fibres can be followed by a milling to half fibre geometry to visualise cracks post-mortem. The crack path mechanism during the test was touched upon in Figs. 7 and 8: multiple scenarios can be outlined. (i) A change in failure mode suggests the cracks propagated in mode II, deflected in the middle of the fibres before reconverting to mode II on the outskirts of the fibre-and-interphase system. (ii) A crack propagating along the fibre/BN interface was arrested at a strongly bonded area, inducing secondary cracks along the BN/matrix interface to propagate next. (iii) Multiple cracks formed simultaneously in weakly bonded zones.

In addition to being able to relate failure mode to micro-structure, the trench push-outs present multiple advantages: the thickness and exact testing length of the fibre can be controlled, the top and bottom of the fibres can be concurrently tracked, the tests can be stopped and/or resumed at any point, and the FIB surface finish surpasses that of the mechanical polishing in quality. The trench push-outs are easy to fabricate, reproducible, and provide clearer visualisation of micro-scale events during the fibre push-out. Trench push-outs also enable further analysis of the effect of thickness/total push-out length on the measured ISS. When compared to traditional fibre push-outs, the new technique inherently transposes multiple dependencies on the number of artefacts around—and in—the fibre (including its unbroken length), to a somewhat unique dependency on unbroken fibre length (because artefacts can be visualised). The problem thus transforms from being both defect-controlled and load-controlled, to only load-controlled (reducing the need for Weibull statistics). The trench push-out being an SEM in-situ test, it ensures that monitoring is done for tip damage, which can occur without being detected during traditional push-out testing of ceramic fibres.

Despite resolving some assumptions of the traditional fibre push-out, trench push-outs present several limitations including the continuing lack of full 3D information, the access to specialised equipment, and the time of milling which can take longer than grinding. Another limitation lies in the uncertainty of milling depth in the trenches, as any inhomogeneity in milling can result in the fibre being pushed out to touch the underlying redeposition material; however, this can be noticed before starting tests. Finally, half fibre trench push-outs are limited by

the precision to which one can section half a fibre; this can be alleviated by measuring the top surface arc length and modifying Eq. (2) equation to account for any custom geometry (as the perimeter of the half fibre may in practise be slightly higher or lower than  $\pi R$ ). The trench push-out nevertheless generated reliable and reproducible results, monitored in real-time.

## Conclusions

A novel trench fibre push-out was introduced for SEM in-situ investigation of interfacial properties in CMCs. The FIB preparation of samples was relatively simple and required no thinning of the samples. The new method further enabled live monitoring of the push-out mechanisms explaining the stochastic nature of its results. The numerical data from calculating frictional interfacial shear stresses on half and full fibres showed reliability and the mechanical properties matched expected trends when comparing the rougher Tyranno type SA3 fibres to the Hi-Nicalon fibres. Failure mechanisms during the fibre push-out were investigated with most fibres showing mixed-mode failure (with simultaneous inside and outside debonding) and some fibres with defective interphases showing linking of smaller cracks before push-out. Transverse cracks in the neighbouring CVI SiC were seen to have propagated before fibre sliding, accompanied by a coiling and resurfacing of the damaged BN interphase. All these micromechanical events were observed leading to potential explanations in the scatter of data acquire from more traditional push-outs. Finally, the benefits and limitations of the trench push-out technique were discussed.

## Methods

Two SiC<sub>f</sub>/BN/SiC composites manufactured by Rolls-Royce High Temperature Composites (Cypress, CA) through a combination of Chemical Vapour Infiltration (CVI) & Melt Infiltration (MI) processes were used as model materials. The two composites differed in their fibre types: Hi-Nicalon™ (COI Ceramics Inc.) and Tyranno SA grade 3\* (Ube Industries Ltd.) of dissimilar fibre radii (7  $\mu\text{m}$  and 5  $\mu\text{m}$ ), and CVI-deposited interphases (200  $\pm$  50 nm and 600  $\pm$  50 nm thicknesses, respectively).

Sample preparation of the trench push-out was performed on the dual SEM–FIB column Zeiss Auriga using milling currents of 4 nA for cutting of the trenches, 2 nA for surface ‘polish’ and 240 pA for surface finish. Micromechanical testing with the trench push-outs was performed both ex-situ and SEM in-situ on a Tyranno type SA3 fibre sample. More information about the ex-situ test is included in the supplementary information.

During in-situ testing, a displacement-controlled speed of 0.1  $\mu\text{m s}^{-1}$  was used on an Alemnis/FEI Quanta FEGSEM column system; images were acquired at 500 ns per frame and a 1024  $\times$  884 resolution. Test were performed on both full and



half Hi-Nicalon fibres on the cross section. The full fibres tests allow tracking of the displacements of the top and bottom fibre surfaces, whereas the half fibre tests allow investigation of cracking along the fibre interfaces.

EDX analysis was performed on a Zeiss Merlin instrument using a 200 pA probe size, 5 keV accelerating voltage and an 8.5 mm working distance—each map was drift corrected and acquired over periods of 30 minutes each. The surface topography was measured by scanning with a Berkovich tip using a Hysitron TI Premier nanoindenter in contact mode. The maps spanned an area of  $10 \times 10 \mu\text{m}$  with a step size of 20 nm. Root-mean squared fibre roughnesses were obtained on sub-maps of  $1.5 \times 4 \mu\text{m}$  areas by a Root-Mean Square analysis with the scanning probe software Gwyddion (Version 2.56).

## Acknowledgments

The authors would like to deeply thank Rolls-Royce plc for funding the project and supplying the composite materials studied in this work. The lead author recognises the help of Olivia De Meyere in assisting with some figures. The authors acknowledge the use of characterisation facilities within the David Cockayne Centre for Electron Microscopy, Department of Materials, University of Oxford, alongside financial support provided by the Henry Royce Institute (Grant ref EP/R010145/1).

## Declarations

**Conflict of interest** The authors declare no conflicts of interest.

## Supplementary Information

The online version contains supplementary material available at <https://doi.org/10.1557/s43578-021-00153-1>.

## Open access

This article is licensed under a Creative Commons Attribution 4.0 International License, which permits use, sharing, adaptation, distribution and reproduction in any medium or format, as long as you give appropriate credit to the original author(s) and the source, provide a link to the Creative Commons licence, and indicate if changes were made. The images or other third party material in this article are included in the article's Creative Commons licence, unless indicated otherwise in a credit line to the material. If material is not included in the article's Creative Commons licence and your intended use is not permitted by statutory regulation or exceeds the permitted use, you will need to obtain permission directly from the copyright holder. To view a copy of this licence, visit <http://creativecommons.org/licenses/by/4.0/>.

## References

1. J. Kabel, P. Hosemann, Y. Zayachuk, D.E.J. Armstrong, T. Koyanagi, Y. Katoh, C. Deck, Ceramic composites: a review of toughening mechanisms and demonstration of micropillar compression for interface property extraction. *J. Mater. Res.* **33**(04), 424 (2018)
2. J.A. DiCarlo. *Advances in SiC/SiC Composites for Aero-Propulsion* (2013)
3. D. Chen, X.-F. Zhang, R.O. Ritchie, Effects of grain-boundary structure on the strength, toughness, and cyclic-fatigue properties of a monolithic silicon carbide. *J. Am. Ceram. Soc.* **83**(8), 2079 (2004)
4. C. Zhen, X. Li, B. Zhang, X. Zhou, C. Liu, Z. Li, Y. Jiang, L. Zhang, L. Cheng, The improvement of mechanical properties of SiC/SiC composites by in situ introducing vertically aligned carbon nanotubes on the PyC interface. *Ceram. Int.* **45**(3), 3368 (2019)
5. G.N. Morscher, H.M. Yun, J.A. DiCarlo, L. Thomas-Ogbuji, Effect of a boron nitride interphase that debonds between the interphase and the matrix in SiC/SiC composites. *J. Am. Ceram. Soc.* **87**(1), 104 (2004)
6. F. Rebillat, J. Lamon, A. Guette, The concept of a strong interface applied to SiC/SiC composites with a BN interphase. *Acta Mater.* **48**(18–19), 4609 (2000)
7. J. Lamon, *Ceramic Matrix Composites* (Wiley, Hoboken, NJ, 2014), pp. 40–64
8. N. Carrère, E. Martin, J. Lamon, The influence of the interphase and associated interfaces on the deflection of matrix cracks in ceramic matrix composites. *Compos. Part A Appl. Sci. Manuf.* **31**(11), 1179 (2000)
9. S. Bertrand, P. Forio, R. Pailler, J. Lamon, Hi-Nicalon/SiC minicomposites with (pPyrocarbon/SiC)<sub>n</sub> nanoscale multilayered interphases. *J. Am. Ceram. Soc.* **82**(9), 2465 (1999)
10. C.-H. Hsueh, Evaluation of interfacial properties of fiber-reinforced ceramic composites using a mechanical properties microprobe. *J. Am. Ceram. Soc.* **76**(12), 3041 (1993)
11. N.P. Bansal, J. Lamon, *Ceramic Matrix Composites: Materials, Modeling and Technology* (Wiley, New York, 2014).
12. D. Hull, T.W. Clyne, *An Introduction to Composite Materials* (Cambridge University Press, Cambridge, 1996).
13. A.F. Kalton, S.J. Howard, J. Janczak-Rusch, T.W. Clyne, Measurement of interfacial fracture energy by single fibre push-out testing and its application to the titanium–silicon carbide system. *Acta Mater.* **46**(9), 3175 (1998)
14. F. Rebillat, J. Lamon, R. Naslain, E. Lara-Curzio, M.K. Ferber, T.M. Besmann, Properties of multilayered interphases in SiC/SiC chemical-vapor-infiltrated composites with “weak” and “strong” interfaces. *J. Am. Ceram. Soc.* **81**(9), 2315 (2005)
15. E.E. Boakye, P. Mogilevsky, T.A. Parthasarathy, K.A. Keller, R.S. Hay, M.K. Cinibulk, Processing and testing of RE<sub>2</sub>Si<sub>2</sub>O<sub>7</sub>

- fiber-matrix interphases for SiC-SiC composites. *J. Am. Ceram. Soc.* **99**(2), 415 (2016)
16. M. Herbreteau, S. Jouannigot, P. Weisbecker, A. Coradi, E. Martin. A New Push-Out Procedure for the Evaluation of Interfacial Properties of SiC/SiC Composites (2012)
  17. M. Desaeger, I. Verpoest, On the use of the micro-indentation test technique to measure the interfacial shear strength of fibre-reinforced polymer composites. *Compos. Sci. Technol.* **48**(1-4), 215 (1993)
  18. W.M. Mueller, J. Moosburger-Will, M.G.R. Sause, S. Horn, Microscopic analysis of single-fiber push-out tests on ceramic matrix composites performed with Berkovich and flat-end indenter and evaluation of interfacial fracture toughness. *J. Eur. Ceram. Soc.* **33**(2), 441 (2013)
  19. O.G. Diaz, K. Marquardt, S. Harris, L. Gale, L. Vandeperre, E. Saiz, F. Giuliani, Degradation mechanisms of SiC/BN/SiC after low temperature humidity exposure. *J. Eur. Ceram. Soc.* **40**(12), 3863 (2020)
  20. J.H. You, W. Lutz, H. Gerger, A. Siddiq, A. Brendel, C. Höschen, S. Schmauder, Fiber push-out study of a copper matrix composite with an engineered interface: experiments and cohesive element simulation. *Int. J. Solids Struct.* **46**(25-26), 4277 (2009)
  21. R. De Meyere, L. Gale, S. Harris, I. Edmons, T.J. Marrow, D.E.J. Armstrong, Optimizing the fibre push-out method to evaluate interfacial failure in SiC/BN/SiC ceramic matrix composites. *J. Am. Ceram. Soc.* (2020). <https://doi.org/10.1111/jace.17673>
  22. W. Yang, A. Kohyama, T. Noda, Y. Katoh, T. Hinoki, H. Araki, J. Yu, Interfacial characterization of CVI-SiC/SiC composites. *J. Nucl. Mater.* **307-311**, 1088 (2002)
  23. M.D. Thouless, Cracking and delamination of coatings. *J. Vac. Sci. Technol. A* **9**(4), 2510 (1991)
  24. E. Buet, C. Sauder, D. Sornin, S. Poissonnet, J.N. Rouzaud, C. Vix-Guterl, Influence of surface fibre properties and textural organization of a pyrocarbon interphase on the interfacial shear stress of SiC/SiC minicomposites reinforced with Hi-Nicalon S and Tyranno SA3 fibres. *J. Eur. Ceram. Soc.* **34**(2), 179 (2014)
  25. C. Sauder, A. Brusson, J. Lamon, Influence of interface characteristics on the mechanical properties of Hi-Nicalon type-S or Tyranno-SA3 fiber-reinforced SiC/SiC minicomposites. *Int. J. Appl. Ceram. Technol.* **7**(3), 291 (2010)
  26. E. Vanswijghoven, K. Lambrinou, M. Wevers, O. Van Der Biest, Comparative study of the surface roughness of Nicalon and Tyranno silicon carbide fibres. *Compos. Part A Appl. Sci. Manuf.* **29**(11), 1417 (1998)
  27. O. Gavalda Diaz, D.A. Axinte, P. Butler-Smith, D. Novovic, On understanding the microstructure of SiC/SiC Ceramic Matrix Composites (CMCs) after a material removal process. *Mater. Sci. Eng. A* **743**, 1 (2019)
  28. N. Jacobson, S. Farmer, A. Moore, H. Sayir, High-temperature oxidation of boron nitride: I, monolithic boron nitride. *J. Am. Ceram. Soc.* **82**(2), 393 (2004)
  29. N.S. Jacobson, G.N. Morscher, D.R. Bryant, R.E. Tressler, High-temperature oxidation of boron nitride: II, boron nitride layers in composites. *J. Am. Ceram. Soc.* **82**(6), 1473 (2004)
  30. C. Wu, R. Huang, K.M. Liechti, Characterizing interfacial sliding of through-silicon-via by nano-indentation. *IEEE Trans. Dev. Mater. Reliab.* **17**(2), 355 (2017)